Helmholtz-Zentrum Dresden-Rossendorf (HZDR)

Wire-Mesh Sensor Super-Resolution Based on Statistical Reconstruction

de Assis Dias, F.; Pipa, D. R.; Morales, R. E. M.; Da Silva, M. J.;

Wire-Mesh Sensor Super-Resolution Based on Statistical Reconstruction

Felipe d. A. Dias, Daniel R. Pipa *Member, IEEE*, Rigoberto E. M. Morales and Marco J. da Silva *Senior Member, IEEE*

Abstract—Wire-mesh sensor (WMS) is an instrument used to visualize and estimate derived parameters of multiphase flows, i.e. gas void fraction and liquid hold-up. Due to its high temporal and spatial resolution, the sensor has been widely applied in the investigation of fluid dynamics. However, the structure of WMS is composed of intrusive electrodes and its image resolution is associated to the number of crossing points formed by the transmitter and receiver wires. In many processes, however, the intrusiveness caused by the electrodes may be a limitation on its use, since they increase the pressure drop and might fragment bubbles depending on the flow condition. Therefore, the reduction of the number of electrodes could probably extend the application field of wire-mesh sensors. Thus, we propose an image reconstruction method to increase resolution of WMS data with fewer wires than most WMS reported in the literature. Hence a reduction of intrusive effects on the process may be achieved. The proposed reconstruction method is based on the Minimum Mean Squared Error (MMSE) estimator. Experimental flow data from a 16×16 WMS are used to produce a Multivariate Gaussian flow model, which in turn is used as regularization in the reconstruction. A sensitive matrix is estimated by finite element method (FEM). Experimental data from two-phase water-gas at slug flow condition are used to validate the proposed method and compared with cubic interpolation. The results show that the MMSE estimator performs better than cubic interpolation and the standard direct problem formulation, reducing the void fraction deviation from 18.20% to 7.92% in the worst case (2×2 WMS).

Index Terms—Inverse problem, multiphase flow, statistical image reconstruction, Wire-Mesh sensor.

I. INTRODUCTION

Multiphase flow occurs in many industrial applications, i.e. distillation columns, bed reactors, production/transportation of oil-gas, etc. In such processes, two or more phases usually streams simultaneously confined to pipes. Thus, the measurement of flow parameters, i.e. liquid hold-up and gas void fraction are extremely important to improve efficiency and to ensure the safety of facilities and processes [1]–[3]. In addition to industrial applications, the use of multiphase-flow-meters (MFM) are also required in scientific studies, for instance, to investigate detailed flow phenomena. Hence accurate MFM is

sought. In this direction, a wide variety of instruments has been designed and successfully applied for both scientific and industrial purposes. In special tomographic flow imaging is desired as it enables the visualization and detailed measurement of the flow [4], e.g. tomographic sensors based on gamma-ray [5], x-ray [6], ultrasound [7], electrical impedance/capacitance [8], [9], among others have been introduced and applied in the past (for an overview see [10]). In the group of instruments based on electrical impedance/capacitance principle, the wire-mesh sensor (WMS) [11], [12] has been applied in several studies and industrial applications, allowing the improvement and validation of models [13].

Although the spatial and temporal resolutions of WMS are considered high, its structure is composed of intrusive electrodes, which is usually manufactured using thin stainless-steel wires stretched over the pipe wall. The resolution of the cross-sectional images provided by the WMS is given by the number crossing points of receiver and transmitter electrodes. In some applications, however, the intrusive effect caused by the wires may be a limitation on its use. Hence a reduction of electrodes could possibly expand the number of application fields of WMS. This strategy however, underestimates derived parameters (i.e. void fraction), if the number of crossing-points is too low (more discussions in the Results section). For this reason, image reconstruction techniques should be employed to ensure the correct measurement of low-resolution WMS data. In this direction, Da Silva [14] and Wagner et al. [15] used field simulation to investigate the spatial sensitivity distribution of the capacitance WMS. They found that the interrogated virtual volume could be affected by perturbations outside its border. Based on this finding, Sun and Wang [16] generated a sensitivity matrix and formulated the capacitance readings of a WMS as an inverse problem. Since this formulation is ill-posed, they used the Conjugate Gradient method with a modified sensitivity matrix to improve the image quality. Ren et al. [17] proposed an approach to improve the image from conductivity WMS. They assumed that images from WMS are almost binary for stratified and annular flow and solved the inverse problem using the Sparse Minimization with Folded Concave Penalty (SMFCP) method. More recently, Sun and Li [18] implemented an algorithm based on the Higher Degree Total Variation (HDTV) to reconstruct images from capacitance WMS. All of those contributions showed good improvements on the image quality. However, the applicability of such methods to improve the phase fraction estimation from sensors with extremely coarse resolution is still not clear and need further investigation.

In this context, we propose a reconstruction method based

on the Minimum Mean Squared Error (MMSE) estimator to increase the resolution of wire-mesh data with fewer electrodes than most WMS reported in the literature. As rule of thumb, a spatial resolution of 2-3 mm has been often employed [13]. For example, for one-inch pipe, a 16×16 sensor is frequently used. In this way, we decreased the number of wires of such sensor to 8×8, 6×6, 4×4 and 2×2 in order to reduce its intrusiveness. Then, the proposed MMSE estimator is applied to improves both final image resolution and the derived parameter: cross-sectional averaged void fraction (α).

It should be declared that this paper reuses some content from thesis [19] with permission.

II. WIRE-MESH SENSOR PRINCIPLE

Wire-mesh sensor (WMS) is an impedance-based sensor for the measurement of multiphase mixtures. In contrast with the electrical capacitance tomography (ECT) [10], where the electrodes have no contact with the flow domain, WMS is composed of wires stretched along the cross section of the tube. Fig. 1a shows a schematic of a 4×4 sensor. The transmitter wires are positioned 90 deg related to the receiver wires. Note from the WMS side view (1b) that the set of transmitter and receiver electrodes are axially spaced by a distance d_z (typically 1-3 mm). Thus, when the first switch (S1) is activated, the respective transmitter electrode is excited, while the others are grounded. In this way, the volume fraction of all crossing points related to the transmitter 1 are interrogated at the same time. Then, the signals are conditioned, converted to digital and stored. Once the sequence is executed for all switches (S1 to S4), an array of ADC signal is obtained. This matrix carries information of at least one electrical property of the fluid (i.e. electrical conductivity or permittivity), which in turn is related to the phase fraction.

The way that the electrical property of the mixture relates to the phase fraction using WMS depends on the excitation signal and the conditioning circuit. For instance, the sensor designed by Prasser [11], interrogates the crossing-points with bipolar signals. The output voltage is acquired only when the temporal response reaches the steady state to ensure that the output is purely resistive. Therefore, the phase fraction is estimated based on the electrical conductivity of the fluid.

In the method proposed by Da Silva [12], [14], the system is excited with a sinusoidal signal with a single and constant frequency (usually in between 1 to 5 MHz). Thus, the measurement of fluids with conductivity up to 100 μs/cm can be approximated as purely capacitive. Thus, the phase fraction is calculated based on the relative permittivity of the mixture ε_x, which in turn allows the measurement of two non-conductive fluids, i.e. oil and air.

Both methods have been successfully used by the scientific, academic and industrial communities for two-phase flow measurement. More recently, dual-modality WMS has been introduced to measure both conductivity and permittivity, allowing the visualization and quantification of water-oil-gas three-phase flow. Reader is referred to [20]–[22] for details.

The intrusiveness of the sensor is usually a worthwhile deal, since the WMS measurement does not need any inverse problem formulation. In order words, the WMS raw data can be converted to phase fraction directly. This approach has been compared to different technologies such as x-ray and high-speed camera [23], [24]. In the comparison with x-ray technology, deviation lower than 10% were reported, which is considered very good result. Therefore, the fact that WMS data processing can be approached as a direct problem gives the sensor robustness and high temporal resolution (up to 10 kHz).

From the point of view of spatial resolution, the readings for each crossing-point are processed and converted to a single pixel of the cross-sectional image (see Fig. 2)). That is, the more crossing points, the greater the spatial resolution. However, increasing the number of electrodes also implies increasing the intrusiveness in the system, which produces two effects for sensors manufactured with thin wires: the first is the increase on pressure drop [11], [25]; second, the wires may fragment or deform bubbles for certain flow regimes [24].

These problems may be critical if the sensor is designed to operate in extreme conditions. In some of these versions, the electrodes are built with rods instead of thin wires in order to make them more robust. However, the intrusiveness effect increases drastically in such configurations [11]. Alternatively, Pietruske [25] proposed a novel WMS layout, where the thin wires can be used even in extreme conditions. In this case, the electrodes are connected and stretched on the sensor wall by springs. This ingenious mechanism ensures the correct operation of the sensor upon high pressure and temperature. In addition, it provides less pressure drop compared to the rod electrodes. However, the mechanical complexity is increased significantly compared to the traditional sensors. More recently, industrial wire-mesh sensor with embedded computing [26] has also been proposed which could also benefit of less intrusiveness by having less electrodes.

In order to attenuate these limitations, we propose in this work a reconstruction method to increase the resolution of wire-mesh sensors (1 in diameter) with very coarse number of electrode wires, i.e. 8×8, 6×6, 4×4 and 2×2. Both low-resolution sensors are then reconstructed to 16×16, which is considered the optimal configuration for 1-inch pipe. Thus, the effects of intrusiveness may be reduced, maintaining the high spatial resolution. We also evaluate the average phase fraction, which is an important derived parameter for many practical applications. Hence, the goal is to improve both resolution and phase fraction in order to expand the range of applicability of the wire-mesh sensor.

III. INVERSE PROBLEM FORMULATION

As explained earlier, the WMS acquisition can be approximated as a direct problem. In this case, it is assumed that the electric field present in the volume interrogated by each crossing-point is homogeneous and bounded by the region d_w (Fig. 2). However, several works have demonstrated by means of the Finite-Element-Method (FEM) that the lines of the electric field extrapolate the virtual area d_w, affecting the measurements of the neighboring crossing-points [14].

Taking into account this non-ideal behavior and based on [14], we created a finite element model of the wire-mesh
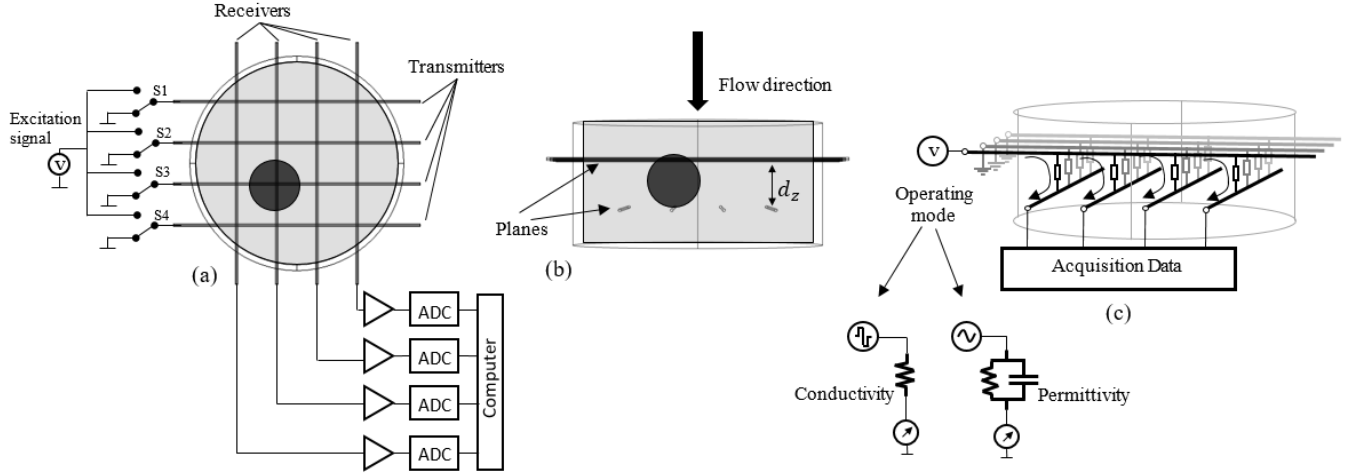
Fig. 1: Scheme of 4×4 Wire-Mesh Sensor: (a) 2D upper view; (b) 2D lateral view; (c) 3D view of WMS. It crossing-point is represented by a virtual complex impedance to emulate the contact of the fluid with transmitter and receiver wires.
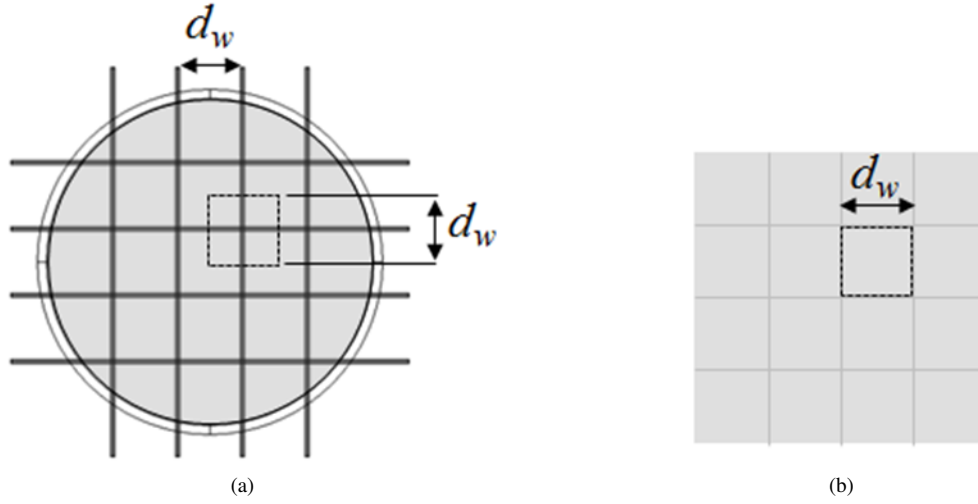

Fig. 2: Wire-mesh sensor visualization by direct problem. (a) Sensitivity area of a crossing-point (square with dashed line); (b) Cross-section visualization. The output signals from each crossing-point are converted to pixels.

sensor to generate a sensitivity matrix $\mathbf{W}$ to increase the resolution of sensors with much less electrodes than the optimal one (Fig. 3).

The procedure for estimating the operator $\mathbf{W}$ was performed in the software COMSOL Multiphysics® using the electrostatic module. In this configuration, the electric field of a 3D WMS model is approximated as a quasi-static problem. It solves the poison equation

$$\nabla(\varepsilon_o \varepsilon(\mathbf{r}) \nabla V(\mathbf{r})) = 0, \tag{1}$$

where, $\mathbf{r}$ is the spatial coordinate, ε_o is the permittivity of vacuum and ε is the relative permittivity of the material.

As in the real sensor procedure, the transmitter electrodes of the model are excited individually, while the others are grounded. The capacitance of the interrogated volume at each crossing-point can be estimated by solving the following surface integral

$$C = \frac{1}{V} \int_{\Gamma} \rho(\Gamma) \cdot d\Gamma, \tag{2}$$

where, V is the voltage, ρ is the charge density and Γ is the surface of the receiver wire.

In order to obtain the sensitivity matrix $\mathbf{W}$, a low-resolution WMS model is segmented according to the resolution of the optimal one. Fig. 3b exemplify this arrangement (4×4 WMS model and 16×16 segments), where the center of each segment matches to the crossing-points of the optimal sensor. The lines of the matrix $\mathbf{W}$ are generated by measuring the disturbance effects produced by each segment. Thus, we used the electrical properties of water as perturbation and the properties of air for the undisturbed points. With this procedure, one obtains

$$\mathbf{W}(i, j) = \frac{C_H(j) - C_x(i, j)}{C_H(j) - C_L(j)}, \tag{3}$$

where, C are the capacitances estimated by (2). The capacitances C_H and C_L are obtained when the whole pipe domain is filled with water and air, respectively. C_x is the capacitance disturbed by a single segment. The indexes j and i are referred
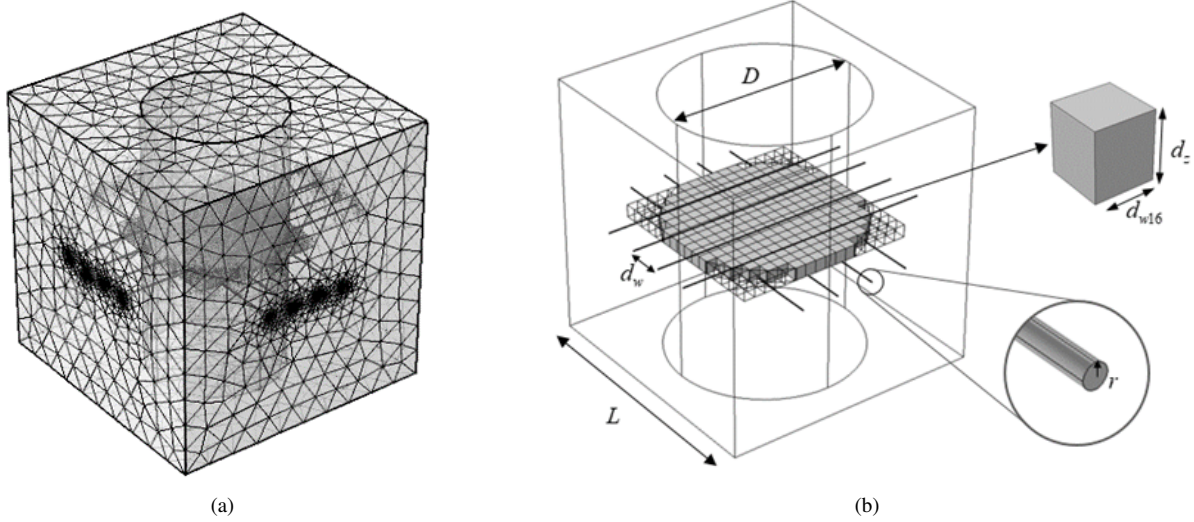
Fig. 3: Finite-element-model of wire-mesh sensor. (a) Mesh of a 4×4 WMS into a squared shape domain. (b) Segmentation based on the 16×16 WMS to generate the sensitivity matrix $\mathbf{W}$.

to the crossing-points related to the high and low-resolution WMS, respectively.

After the sensitivity matrix is obtained, the WMS acquisition can be modelled as

$$\mathbf{g} = \mathbf{W}\mathbf{f} + \boldsymbol{\nu}, \qquad (4)$$

where $\mathbf{g}$ is the observation, W is the sensitivity matrix, $\mathbf{f}$ is the high-resolution image and $\boldsymbol{\nu}$ is the measurement noise. The goal is to calculate the high-resolution image $\mathbf{f}$ from the low-resolution observation $\mathbf{g}$. Thus, $\mathbf{f}$ can be estimated as an inverse problem formulation, for instance, by solving the *linear back projection* (LBP)

$$\hat{\mathbf{f}} = \mathbf{W}^T \mathbf{g}, \qquad (5)$$

or, the *minimum-norm*

$$\hat{\mathbf{f}} = \mathbf{W}^T (\mathbf{W}\mathbf{W}^T)^{-1} \mathbf{g}. \qquad (6)$$

Fig. 4 shows the estimation of $\mathbf{f}$ using both algorithms to a single WMS frame. Note that all solutions estimated by (5) and (6) give poor results. It happens because the system is highly underdetermined. In addition, the sensitivity matrix is sparse and does not provide enough information when the number of WMS electrodes are extremely coarse. Therefore, we propose a reconstruction method based on the Minimum Mean Squared Error (MMSE) estimator. It can be solved as

$$\hat{\mathbf{f}} = (\mathbf{W}^T\mathbf{W} + \sigma_{\boldsymbol{\nu}}^2 \boldsymbol{\Sigma}_{\mathbf{f}}^{-1})^{-1} (\mathbf{W}^T\mathbf{g} + \sigma_{\boldsymbol{\nu}}^2 \boldsymbol{\Sigma}_{\mathbf{f}}^{-1} \boldsymbol{\mu}_{\mathbf{f}}). \qquad (7)$$

Here, the regularization by a Multivariable Gaussian Model (MGM) is used to increase the resolution of WMS data. The sensitivity matrix $\mathbf{W}$ can be found by Finite Element Method (FEM), as discussed previously. The statistical parameters (mean and covariance) can be estimated through experimental flow data. Finally, the variance of the measuring noise, which is often rewritten as a regularization factor λ, can be adjusted

experimentally. The reader is referred to [27], [28] for the complete demonstration.

Eq. (7) can also be rearranged by using the Matrix Inversion Lemma [27] as follows

$$\hat{\mathbf{f}} = \boldsymbol{\mu}_{\mathbf{f}} + \boldsymbol{\Sigma}_{\mathbf{f}}\mathbf{W}^T (\mathbf{W}\boldsymbol{\Sigma}_{\mathbf{f}}\mathbf{W}^T + \lambda\mathbf{I})^{-1}(\mathbf{g} - \mathbf{W}\boldsymbol{\mu}_{\mathbf{f}}). \qquad (8)$$

Note that (7) and (8) are equivalents. However, (8) is preferably since the sensitivity matrix $\mathbf{W}$ do not need to be full rank to ensure that the term $(\mathbf{W}\boldsymbol{\Sigma}_{\mathbf{f}}\mathbf{W}^T + \lambda\mathbf{I})$ is invertible.

IV. METHODOLOGY

A. Experimental setup

The statistical parameters to regularize the proposed reconstruction method were obtained experimentally in a multiphase flow facility. The setup is a water-gas two-phase flow loop located at the NUEM (*Núcleo de Escoamento Multifásico*) at the *Federal University of Paraná*. Fig. 5 shows the schematic of the plant. It consists of a horizontal section of acrylic tube of 26 mm inner diameter and 9 m long. Tap water and air are injected into the system through a mixer. The water flow rate is monitored by a Coriolis-flow meter and controlled by a pump connected to a frequency inverter. The air phase is monitored by a rotameter and controlled manually by a valve. The readings of the flow rate and the control of the frequency inverter were performed with a user interface in LabVIEW®. The horizontal pipe section is connected to the tank, where the air flows out to the atmosphere and the water is reused.

Two wire-mesh sensors were positioned at a distance of 8 m from the mixer to ensure that the two-phase flow is fully developed. All experiments were carried out by placing a high-resolution sensor upstream (Fig. 6f), while a second low-resolution one (Fig. 6b to 6e) was positioned separated by a 2.3 cm thick acrylic flange downstream, as shown in Fig. 5. The readings of both sensors capture the flow dynamics in
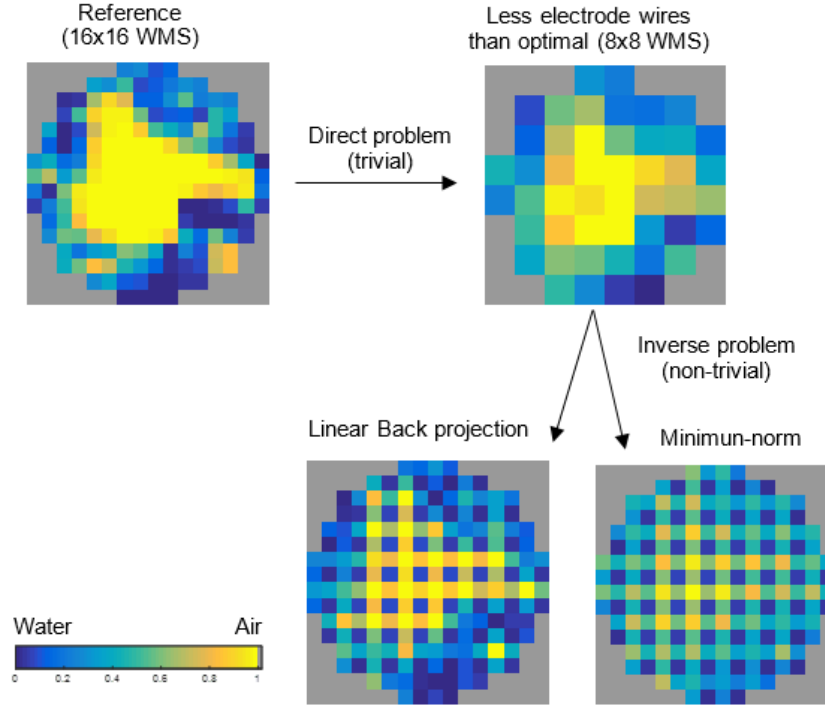
Fig. 4: Direct and inverse problem solved by linear back projection and minimum-norm.
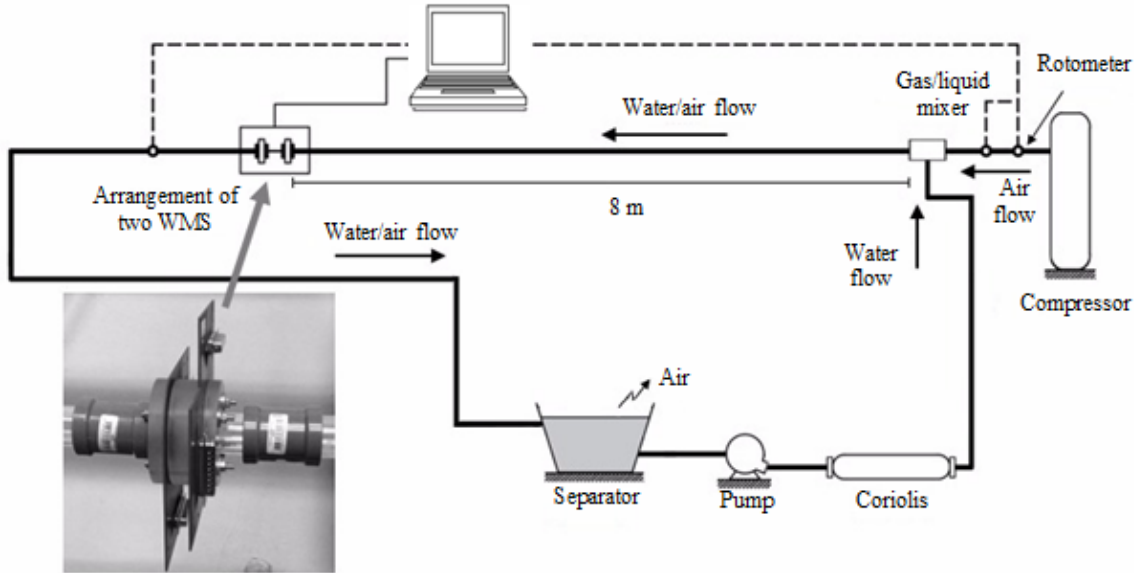

Fig. 5: Schematic of the flow loop used to perform water-air two-phase flow experiments.

similar conditions, but shifted in time. Therefore, the cross-correlation method was used to compensate the time delay of both signals for a better visualization.

B. Operation points

The experiments were carried out at 13 operation points (different pairs of gas j_G and liquid j_L superficial velocities). WMS readings were acquired at a frequency of 2 kHz for 60 s each. Fig. 7 shows a flow pattern map with the operating

points. Note that water and gas superficial velocities (i.e. flow rates) were set to produce intermittent flow. However, although the boundaries of the map are represented by lines, the transition between a given flow regime to another one is not sharp [29]. Therefore, the upper operating points can be eventually be the transition between slug and bubble flow.

C. Data processing for void fraction calculation

The capacitance wire-mesh sensor raw data are voltage signals proportional to the electrical permittivity ε of the fluid
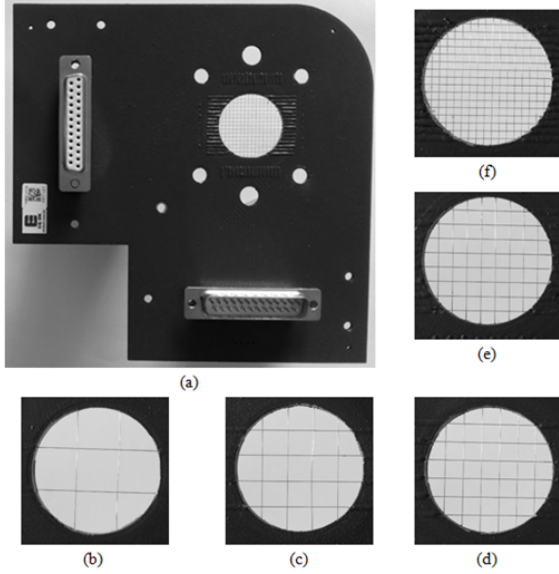
Fig. 6: Wire-mesh sensors with standard resolution (a) 16×16, and reduced number of electrode wires (b) 2×2 (c) 4×4 (d) 6×6 (e) 8×8 (f) 16×16.

in the interrogation volume, which in turn may be calibrated and converted to phase fraction using a proper dielectric mixture model (the reader is referred to [12]).

According to Da Silva et al. [30], the logarithmic model has provided better results for some specific flow conditions, for instance, when the phase distribution contains partially continuous phase and small interfaces (bubbles or droplets), which is the case of the transition of slug/plug to bubble flow. This finding is based on experimental comparisons between WMS and quick-closing valves (QCV) for water-oil two-phase flow. Although the experiments of the present work were performed with water-air mixture, it is reasonable to make the same assumption, since the operating points upon investigation are geometrically similar to those presented in [30]. A benefit of this approach is the fact that the conditioning circuit of a standard capacitance WMS already includes a logarithmic demodulator, which allows compressing the high dynamic range of signals. This feature makes possible the measurement of fluids with large permittivity contrast, such as water, oil and air. Since the measured voltage outputs of WMS are already logarithmic signals (proportional to ε), the void fraction (based on logarithmic permittivity mixture model) can be directly estimated as

$$\alpha(i,j,k) = \frac{V_{\log}^{H}(i,j) - V_{\log}^{M}(i,j,k)}{V_{\log}^{H}(i,j) - V_{\log}^{L}(i,j)}, \tag{9}$$

where $V_{\log}^{M}$ is the measurement, $V_{\log}^{H}$ and $V_{\log}^{L}$ are the output signals when the sensor is filled up with the highest and lowest permittivity medium, respectively (water and air in this work), (i,j) denote the spatial indices over pipe cross section and k is the temporal index.

D. Statistical parameters

In order to solve the inverse problem through the MMSE algorithm, *a priori* information of the flow was obtained experimentally from a single operating point, where the slug flow is well developed (point P7, see Fig. 7. The experiment was performed using the optimal 16×16 WMS (Fig. 6f). Here, we assumed that the frame $\mathbf{f}$ is a random Gaussian vector described as

$$\mathbf{f} \sim N(\boldsymbol{\mu}_{\mathbf{f}}, \boldsymbol{\Sigma}_{\mathbf{f}}), \tag{10}$$

where, $\boldsymbol{\mu}_{\mathbf{f}}$ to $\boldsymbol{\Sigma}_{\mathbf{f}}$ are the mean and covariance, respectively, and estimated by

$$\boldsymbol{\mu}_{\mathbf{f}} = \frac{1}{n} \sum_{i=1}^{n} \mathbf{f}_i, \tag{11}$$

and

$$\boldsymbol{\Sigma}_{\mathbf{f}} = \frac{1}{n-1} \sum_{i=1}^{n} (\mathbf{f}_i - \boldsymbol{\mu}_{\mathbf{f}})(\mathbf{f}_i - \boldsymbol{\mu}_{\mathbf{f}})^{T}, \tag{12}$$

where $\mathbf{f}_i$ are WMS measurements. Fig. 8 show the covariance and mean matrices obtained experimentally from the operating point P7.

V. RESULTS

Fig. 9 shows the temporal void fraction of one selected operating point acquired with the low-resolution 8×8, 6×6, 4×4, 2×2 and the optimal 16×16 WMS. As can be seen, the void fraction generated by the low-resolution sensor deviates from the optimal one when the number of electrodes is reduced. As expected, this problem is accentuated if the sensor resolution is extremely coarse (2×2). However, by using the MMSE algorithm, the void fraction deviation is attenuated.

A. Quantitative results

In order to evaluate the results quantitatively, we calculated the absolute deviation of the average void fraction for the following methods: (a) directed problem, (b) cubic interpolation (function *interp2* from Matlab®) and (c) the proposed method MMSE. Fig. 10 shows the results for all operating points. As can be seen, the proposed method MMSE presents a maximum deviation less than 5% for 8×8 and 6×6 WMS. In contrast, the direct problem and the interpolation gave an absolute deviation up to 10.99%.

When the WMS resolution is extremely coarse, i.e. 4×4 and 2×2, the MMSE algorithm presented deviation up to 7.92%. On the other side, the interpolation and direct problem underestimate the void fraction even more, reaching a deviation up to 18.20%.

The void fraction depreciation occurs because the presence of bubbles much smaller than the WMS resolution. Thus, the deviation is obviously increased when the number of electrodes are reduced. However, the proposed reconstruction algorithm MMSE was able to compensate it even in the WMS with very coarse resolution. Since the flow streams into a horizontal pipe, the air phase tends to flow in the top of the tube. Thus, the *a priori* information obtained experimentally and used as regularization acts giving different weights to the
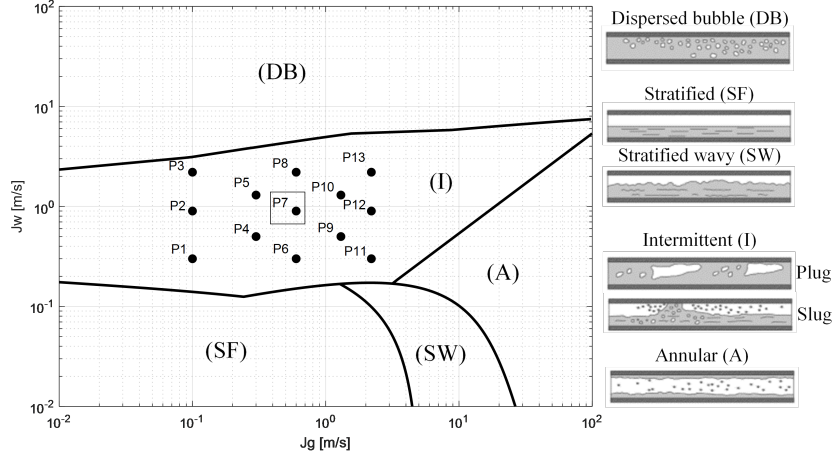
Fig. 7: Horizontal two-phase flow pattern map [29] and the 13 experimental points. The point P7 is used to obtain the statistical parameters for the regularization of the inverse problem.
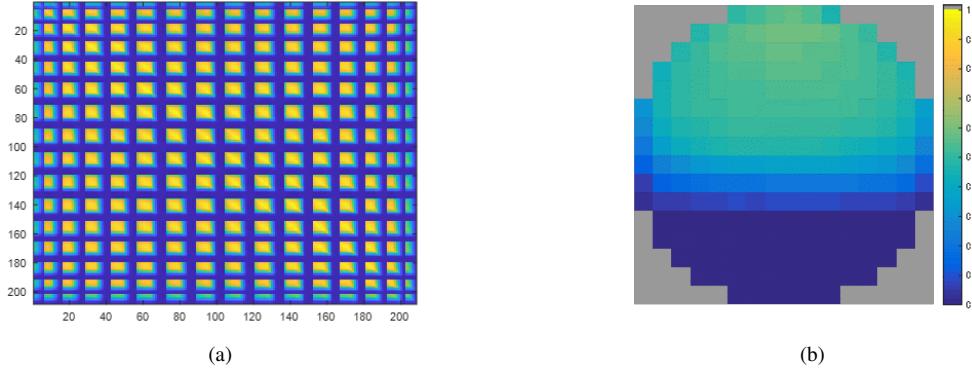

Fig. 8: Statistical parameters obtained experimentally from the operating point P7. (a) Covariance; (b) Mean.

air-related signals present at the upper and lower crossing-points. In this way, the reconstruction algorithm compensates the lack of information due to the small interfaces that could not be measured by the lower resolution sensors. From Fig. 10, it can be also observed that the interpolation method did not provide significant changes on the void fraction compared with the direct problem solution, since obviously there is no extra information available neither from the flow nor from the physical principle of the sensor.

B. Flow visualization

The WMS data can be processed to generate virtual side view of the flow. This type of view is relevant for the investigation of fluid dynamics, e.g. to track or estimate the volume of bubbles. Fig. 11 and 12 illustrate the virtual sectional view of the operating points P12 and P13, respectively. From both flow conditions, it is evident that the MMSE and the interpolation methods produces similar images to the reference when used to reconstruct 8×8 and 6×6 WMS data. However, the MMSE is much more effective than the cubic interpolation when the low-resolution sensor has a very coarse number of electrode wires.

In Fig. 13, it is shown some cross-sectional views of a selected data. Here, it is observed that the proposed method produces sharp images. In contrast, the cubic interpolation suffers with blurring and underestimate the void fraction due to the lack of information, as discussed previously. Since the MMSE algorithm encompasses the characteristics of the electric field with the sensitivity matrix $\mathbf{W}$ (obtained numerically) and *a priori* information of the flow (obtained experimentally), the reconstruction provides details of the flow that cannot be achieved with the direct problem or interpolation. Note that the nose and tail of the gas elongated bubbles presented much more details.

VI. CONCLUSION

In this paper, a new methodology to reconstruct images of very coarse wire-mesh sensor resolution is proposed. The WMS reconstruction is formulated as an inverse problem using the MMSE algorithm. Statistical parameters, i.e. mean and covariance, were obtained experimentally from high-resolution WMS data and used as *a priori* information to reconstruct the low-resolution data.
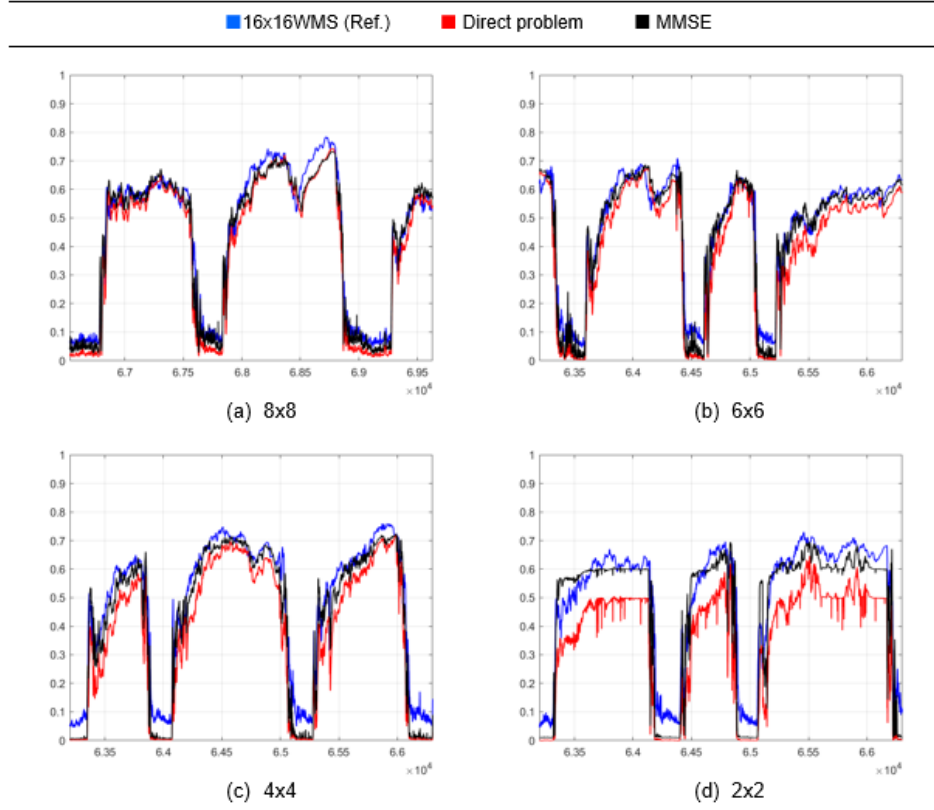
Fig. 9: Time-series void fraction of the selected operating point P12. (Blue) referece 16×16 WMS; (Red) low-resolution WMS; (Black) reconstructed data by MMSE.
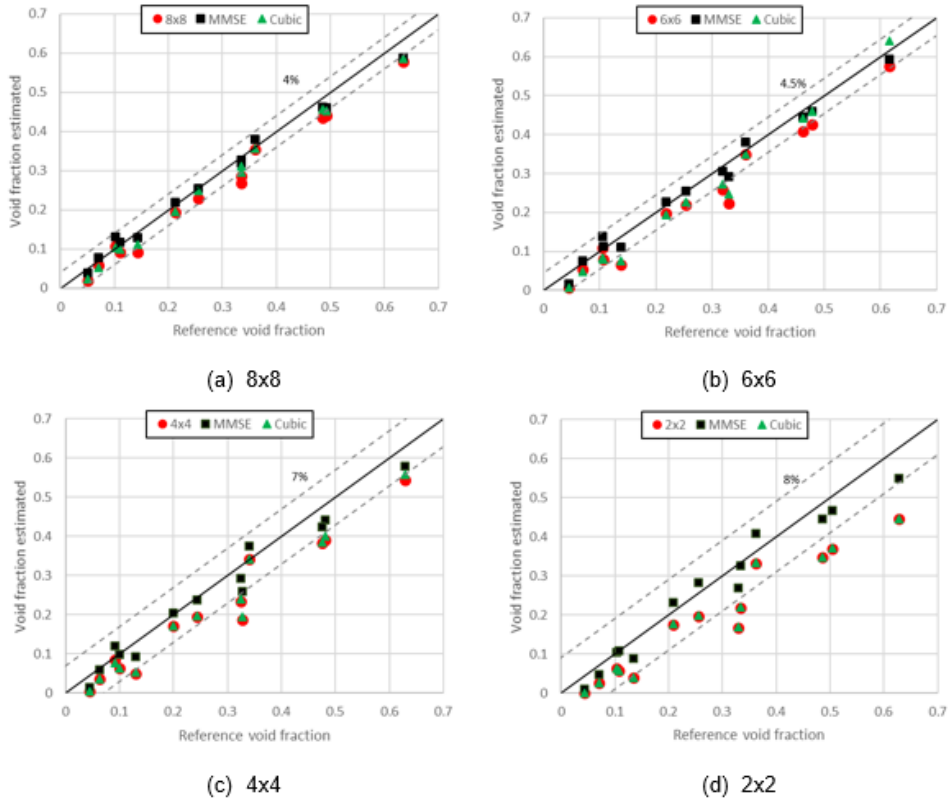

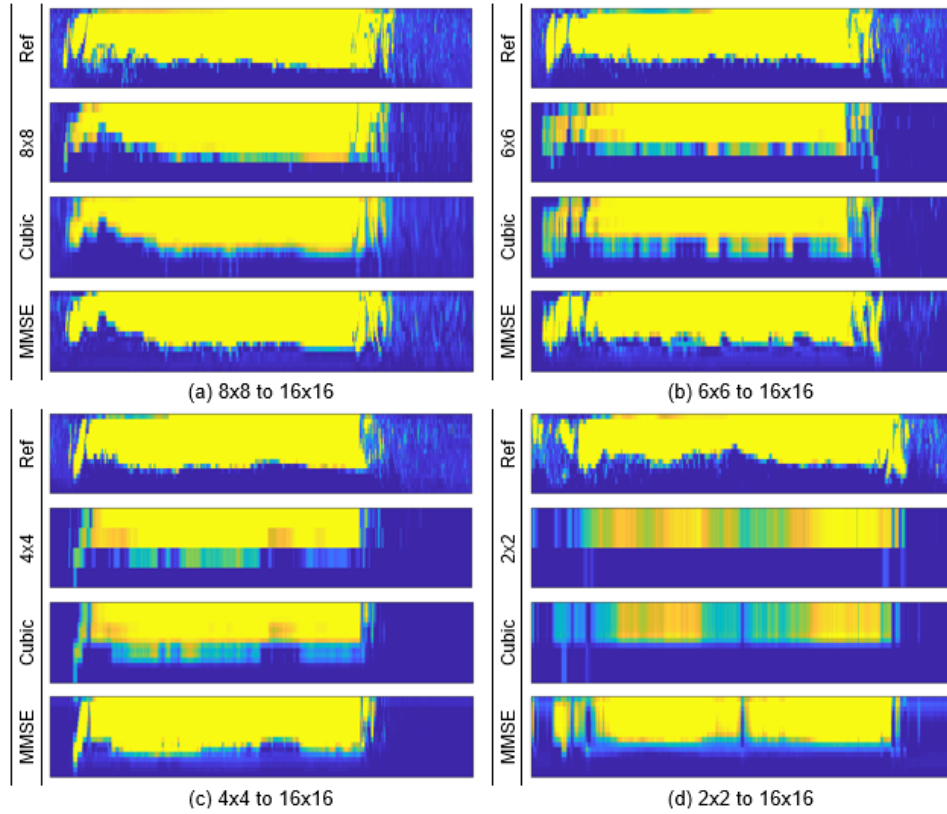Fig. 10: Absolute deviation of the average void fraction.

Fig. 11: Virtual side view of the operating point P11. (Ref) is the high-resolution image from the 16×16 wire-mesh sensor and (Low) is the low-resolution image reconstructed by the cubic interpolation and MMSE.

The results suggest that MMSE algorithm is effective even in the worst case (2×2 WMS), where the image resolution of 13 operating points were increased to 16×16. All points kept deviation less than 7.92% on the average void fraction. In contrast, the interpolation and the direct problem formulation achieved deviation up to 18.20%. Hence, images and void fraction are obtained with high quality from very coarse resolution data while the intrusiveness of the sensor is significantly reduced.

REFERENCES

[1] G. Falcone, G. Hewitt, and C. Alimonti, *Multiphase flow metering: principles and applications*. Elsevier: Amsterdam, The Netherlands, 2009, vol. 54.
[2] L. S. Hansen, S. Pedersen, and P. Durdevic, "Multi-phase flow metering in offshore oil and gas transportation pipelines: Trends and perspectives," *Sensors*, vol. 19, no. 9, 2019.
[3] E. Dahl, C. Michelsen *et al.*, "Handbook of multiphase flow metering," *NFOGM & Tekna*, 2005.
[4] J. Yao and M. Takei, "Application of process tomography to multiphase flow measurement in industrial and biomedical fields: A review," *IEEE Sensors Journal*, vol. 17, no. 24, pp. 8196–8205, 2017.
[5] B. T. Hjertaker, S. . Tjugum, E. A. Hammer, and G. A. Johansen, "Multimodality tomography for multiphase hydrocarbon flow measurements," *IEEE Sensors Journal*, vol. 5, no. 2, pp. 153–160, 2005.
[6] A. Bieberle, D. Windisch, K. Iskander, M. Bieberle, and U. Hampel, "A smart multi-plane detector design for ultrafast electron beam x-ray computed tomography," *Sensors*, vol. 20, no. 18, 2020.
[7] H. Liu, S. Zhao, C. Tan, and F. Dong, "A bilateral constrained image reconstruction method using electrical impedance tomography and ultrasonic measurement," *IEEE Sensors Journal*, vol. 19, no. 21, pp. 9883–9895, 2019.
[8] M. Darnajou, A. Dupré, C. Dang, G. Ricciardi, S. Bourennane, C. Bellis, and S. Mylvaganam, "High speed eit with multifrequency excitation using fpga and response analysis using fdm," *IEEE Sensors Journal*, vol. 20, no. 15, pp. 8698–8710, 2020.
[9] A. d. N. Wrasse, T. P. Vendruscolo, E. N. dos Santos, D. R. Pipa, H. L. de Moura, F. C. Castaldo, R. E. M. Morales, and M. J. da Silva, "Capacitive multielectrode direct-imaging sensor for the visualization of two-phase flows," *IEEE Sensors Journal*, vol. 17, no. 24, pp. 8047–8058, 2017.
[10] M. Wang, *Industrial tomography: systems and applications*. Elsevier, 2015.
[11] H.-M. Prasser, A. Böttger, and J. Zschau, "A new electrode-mesh tomograph for gas–liquid flows," *Flow measurement and instrumentation*, vol. 9, no. 2, pp. 111–119, 1998.
[12] M. Da Silva, E. Schleicher, and U. Hampel, "Capacitance wire-mesh sensor for fast measurement of phase fraction distributions," *Measurement Science and Technology*, vol. 18, no. 7, p. 2245, 2007.
[13] H.-M. Prasser, "Novel experimental measuring techniques required to provide data for cfd validation," *Nuclear Engineering and Design*, vol. 238, no. 3, pp. 744–770, 2008.
[14] M. J. Da Silva, "Impedance sensors for fast multiphase flow measurement and imaging," 2008.
[15] M. Wagner, M. da Silva, S. Thiele, and U. Hampel, "Simulation-based investigation of spatial sensitivity distribution of wire-mesh sensors." Proceedings of Comsol Comference, 2008.
[16] Q. Sun and H. Wang, "Mesh wire tomography combined with a modified sensitivity map," in *2011 IEEE International Conference on Imaging Systems and Techniques*, 2011, pp. 74–78.
[17] S. Ren, H. Liu, C. Tan, and F. Dong, "Tomographic wire-mesh imaging of water-air flow based on sparse minimization," *IEEE Sensors Journal*, vol. 17, no. 24, pp. 8187–8195, 2017.
[18] K. Sun and Y. Li, "An hdtv-sb imaging algorithm for wire-mesh tomography," *Measurement Science and Technology*, vol. 31, no. 4, p. 045404, 2020.
[19] F. d. A. Dias, "Increasing image resolution for wire-mesh sensor based on statistical reconstruction," Master's thesis, Universidade Tecnológica Federal do Paraná, Brazil, 2017.
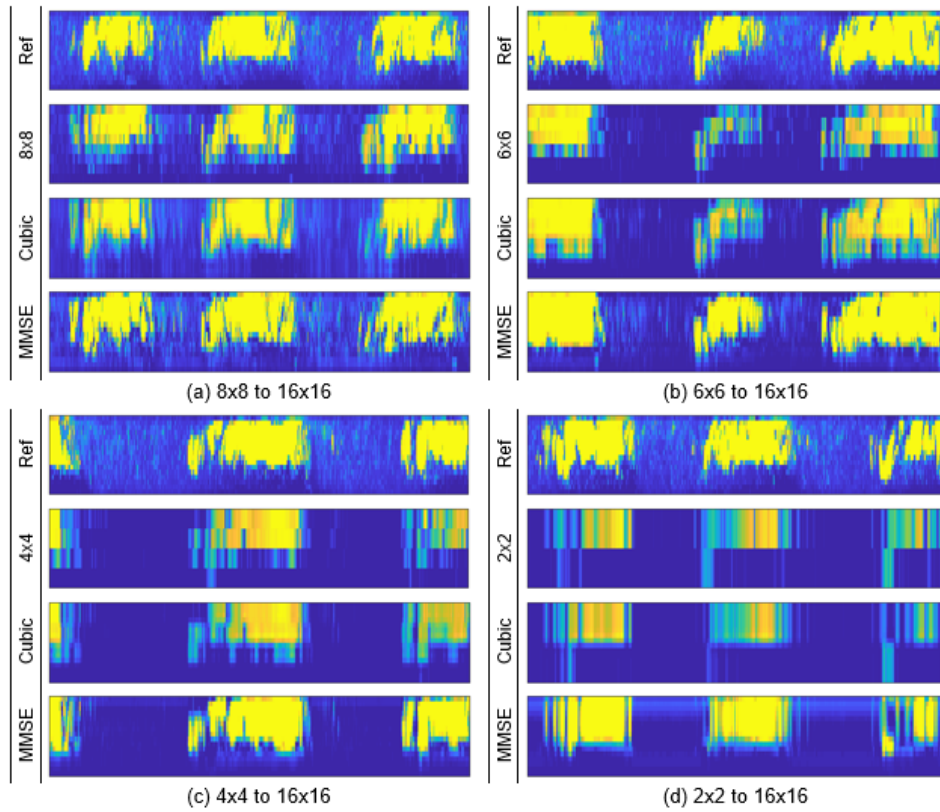
Fig. 12: Virtual side view of the operating point P12. (Ref) is the high-resolution image from the 16×16 wire-mesh sensor and (Low) is the low-resolution image reconstructed by the cubic interpolation and MMSE.

[20] E. N. dos Santos, T. Vendruscolo, R. Morales, E. Schleicher, U. Hampel, and M. Da Silva, "Dual-modality wire-mesh sensor for the visualization of three-phase flows," *Measurement Science and Technology*, vol. 26, no. 10, p. 105302, 2015.

[21] E. N. dos Santos, M. J. da Silva, R. E. Morales, S. Reinecke, E. Schleicher, and U. Hampel, "Dual-modality impedance wire-mesh sensor for investigation of multiphase flows," in *2014 IEEE International Conference on Imaging Systems and Techniques (IST) Proceedings*. IEEE, 2014, pp. 316–319.

[22] F. d. A. Dias, E. N. Dos Santos, M. J. Da Silva, E. Schleicher, R. E. Morales, B. Hewakandamby, and U. Hampel, "New algorithm to discriminate phase distribution of gas-oil-water pipe flow with dual-modality wire-mesh sensor," *IEEE Access*, 2020.

[23] H.-M. Prasser, M. Misawa, and I. Tiseanu, "Comparison between wire-mesh sensor and ultra-fast x-ray tomograph for an air–water flow in a vertical pipe," *Flow Measurement and Instrumentation*, vol. 16, no. 2-3, pp. 73–83, 2005.

[24] H.-M. Prasser, D. Scholz, and C. Zippe, "Bubble size measurement using wire-mesh sensors," *Flow measurement and Instrumentation*, vol. 12, no. 4, pp. 299–312, 2001.

[25] H. Pietruske and H.-M. Prasser, "Wire-mesh sensors for high-resolving two-phase flow studies at high pressures and temperatures," *Flow Measurement and Instrumentation*, vol. 18, no. 2, pp. 87–94, 2007.

[26] R. Kipping, R. Brito, E. Scheicher, and U. Hampel, "Developments for the application of the wire-mesh sensor in industries," *International Journal of Multiphase Flow*, vol. 85, pp. 86–95, 2016.

[27] S. M. Kay, *Fundamentals of statistical signal processing*. Prentice Hall PTR, 1993.

[28] A. C. Bovik, *Handbook of image and video processing*. Academic press, 2010.

[29] Y. Taitel and A. E. Dukler, "A model for predicting flow regime transitions in horizontal and near horizontal gas-liquid flow," *AIChE journal*, vol. 22, no. 1, pp. 47–55, 1976.

[30] M. Da Silva, E. Dos Santos, U. Hampel, I. Rodriguez, and O. Rodriguez, "Phase fraction distribution measurement of oil–water flow using a capacitance wire-mesh sensor," *Measurement Science and Technology*, vol. 22, no. 10, p. 104020, 2011.
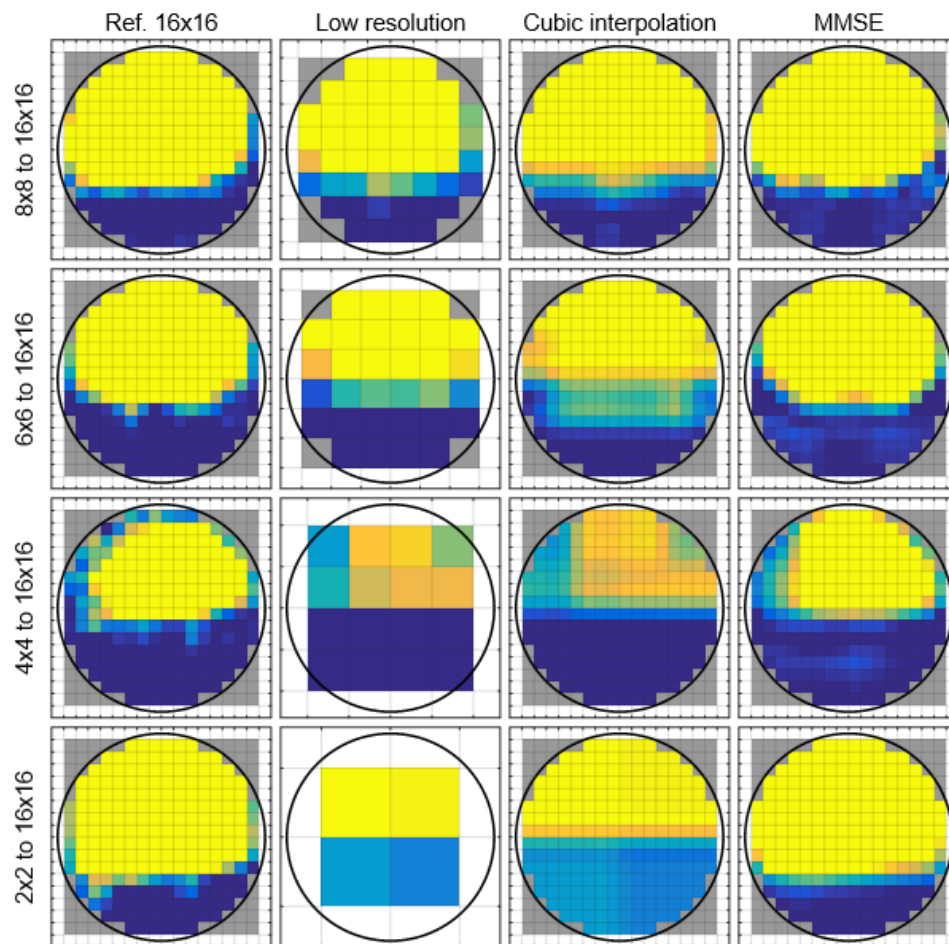
Fig. 13: Selected cross-sectional images from the operating point P11.